Nanoscale Res Lett (2008) 3:421–426
DOI 10.1007/s11671-008-9172-y

NANO EXPRESS

FTIR and Raman Spectroscopy of Carbon Nanoparticles in SiO_2, ZnO and NiO Matrices

G. Katumba · B. W. Mwakikunga · T. R. Mothibinyane

Received: 25 July 2008 / Accepted: 11 September 2008 / Published online: 1 October 2008

Abstract Coatings of carbon nanoparticles dispersed in SiO_2, ZnO and NiO matrices on aluminium substrates have been fabricated by a sol–gel technique. Spectrophotometry was used to determine the solar absorptance and the thermal emittance of the composite coatings with a view to apply these as selective solar absorber surfaces in solar thermal collectors. Cross-sectional high resolution transmission electron microscopy (X-HRTEM) was used to study the fine structure of the samples. Raman spectroscopy was used to estimate the grain size and crystallite size of the carbon clusters of the composite coatings. X-HRTEM studies revealed a nanometric grain size for all types of samples. The C–SiO_2, C–ZnO and C–NiO coatings contained amorphous carbon nanoparticles embedded in nanocrystalline SiO_2, ZnO and NiO matrices, respectively. Selected area electron diffraction (SAED) showed that a small amount of Ni grains of 30 nm diameter also existed in the NiO matrix. The thermal emittances of the samples were 10% for C–SiO_2, 6% for the C–ZnO and 4% for the C–NiO samples. The solar absorptances were 95%, 71% and 84% for the C–SiO_2, C–ZnO and C–NiO samples, respectively. Based on these results, C–NiO samples proved to have the best solar selectivity behaviour followed by the C–ZnO, and last were the C–SiO_2 samples. Raman spectroscopy studies revealed that both the C–ZnO and C–NiO samples have grain sizes for the carbon clusters in the range 55–62 nm and a crystallite size of 6 nm.

Keywords FTIR spectroscopy · Raman spectroscopy · Carbon nanoparticles · Oxide matrices

G. Katumba (✉) · T. R. Mothibinyane
CSIR—National Laser Centre, Building 46A, P.O. Box 395, Pretoria 0001, South Africa
e-mail: gkatumba@csir.co.za

B. W. Mwakikunga
CSIR—National Centre for Nano-Structured Materials, Building 19B, P.O. Box 395, Pretoria 0001, South Africa

B. W. Mwakikunga
School of Physics, University of the Witwatersrand, P O Wits 2050, Johannesburg, South Africa

B. W. Mwakikunga
Department of Physics, University of Malawi, The Polytechnic, P/B 303, Chichiri, Blantyre 3, Malawi

Introduction

The original infrared spectroscopy instruments were of the dispersive type in which prisms and gratings were used to separate the individual frequencies of energy from the infrared source. From the 1980s Fourier transform infrared (FTIR) spectroscopy has been preferred [1] to the old dispersive infrared technologies. The main advantages of FTIR spectroscopy are: non-destructive technique, increased speed of collection of spectra, increased sensitivity with high resolution capability, increased optical throughput and mechanical simplicity.

Raman spectroscopy has been in existence since the late 1920s. It is a technique that is used for material analysis as a complement to infrared spectroscopy. Raman spectroscopy has been applied for the identification of a wide variety of compounds of pigments, minerals, drugs, etc. [2–4]. Lately, portable Raman spectrometers have been demonstrated as useful forensic and security tools for the rapid detection of illicit drugs at airports [5].

In the work reported here, we have used FTIR and Raman spectroscopy techniques to analyse the behaviour of carbon nanoparticles embedded in three different oxide

matrices, namely SiO_2, ZnO and NiO, intended for selective solar absorber applications in solar thermal collectors.

Experimental

The C–SiO_2, C–ZnO and C–NiO samples were prepared by sol–gel techniques whose details are presented elsewhere [6, 7]. FTIR reflectance spectroscopy studies were performed on the samples using a Bomem DA8 spectrometer in the near infrared and the infrared wavelength ranges (2.5–20 μm) and a Lambda 900 spectrophotometer in the ultraviolet and visible wavelength ranges (0.3–2.5 μm). Raman spectroscopy was also used to study these samples using a Jobin-Y von T64000 Raman spectrometer. The observations from the FTIR and Raman spectroscopy studies have been corroborated, wherever possible, by structural analysis techniques such as transmission electron microscopy (TEM), cross-sectional high resolution transmission electron microscopy (X-HRTEM), and selected area electron diffraction (SAED).

Results and Discussion

FTIR Spectroscopy

Figure 1a shows the variation of total reflectance with the amount of carbon precursor (SUC) of C–SiO_2 samples. The investigation was done with 6, 9, 11 and 12 g of SUC for a fixed TEOS: H_2O ratio of 12:9. The low to high reflectance transition appears to move towards an apparent limit of 2 μm with increasing amount of SUC.

It is striking that for wavelengths less than 0.8 μm, the reflectance increased with increasing amount of SUC. It was expected that an increase in SUC would lead to higher absorption, and hence lower reflectance, in the UV–VIS interval. This behaviour suggests that when the amount of SUC is low the resultant carbon chains in the silica matrix have on average a small size and more uniform distribution, as suggested by X-HRTEM image in Fig. 2a, and therefore would have a higher absorption cross section. When the amount of SUC was increased the resultant carbon chains agglomerated to form larger aggregates, as shown in Fig. 2b, with a large scattering cross section that resulted in higher reflectance. The gain in absorptance in the UV–VIS for the low SUC samples was accompanied by a loss in absorptance in the 0.8–2.0 μm interval due to resonance absorption by water molecules.

In the near infrared (NIR) and infrared (IR) regions, the reflectance of the samples with low SUC content is higher than that of samples with higher SUC content. The reason for this is that samples of low SUC content were thinner than those of higher SUC content. This is thought to be purely a viscosity effect of the sol during the spin-coating process. The net result of this behaviour is a lower thermal emittance by samples with low SUC content. It was thus clear that an optimum of SUC content had to be sought. The optimum for samples with high absorptance and low emittance was observed to be 11 g SUC based on the graphs in Fig. 1a.

Characteristic chemical bonds in the C–SiO_2 samples were identified from the FTIR reflectance spectrum presented in Fig. 1b. Three distinct absorption bands are observed. The major band at approximately 1,050 cm^{-1} is assigned to stretching vibrations of Si–O–Si or Si–O–X, where X represents ethoxy groups bonded to silicon [8, 9]. The shoulder at about 1,200 cm^{-1} is assigned to either the transverse optical mode of the out of phase mode of the asymmetric vibration or to the longitudinal optical mode of the high frequency vibration of SiO_2 [8]. On the other side of the major absorption band, at 900 cm^{-1}, is an absorption band that can be assigned to the stretching vibration of Si–OH or Si–O^- groups. A broad absorption band, situated between 3,000 and 3,600 cm^{-1}, and another one around 1,600 cm^{-1} are assigned to O–H stretching and O–H bending vibrations, respectively [8, 9]. The latter

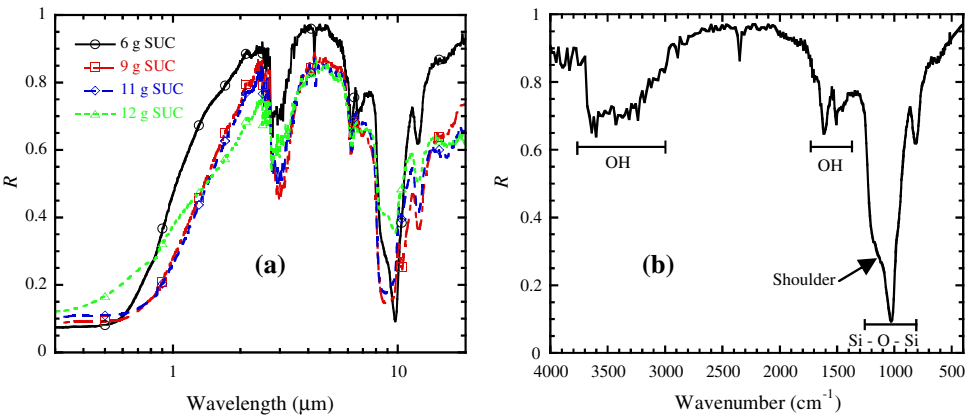

Fig. 1 **a** Effect of the amount of SUC in C–SiO_2 samples spin-coated at 4,000 rpm and **b** identification of chemical bonds in the absorber composite layer from an FTIR reflectance spectrum

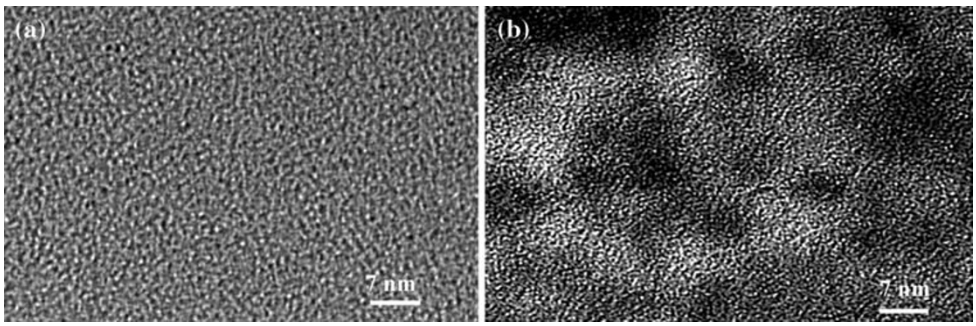

Fig. 2 X-HRTEM images of samples with **a** TEOS only and **b** Ac_2O additive

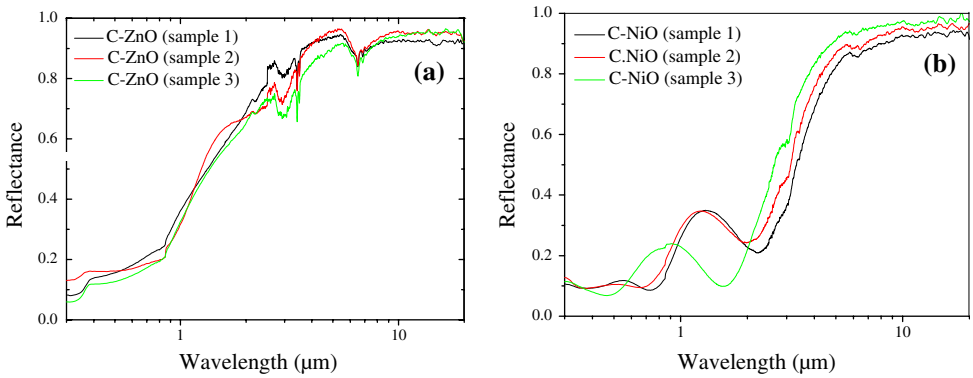

Fig. 3 The near normal reflectance spectra of **a** C–ZnO samples showing a not-so-steep transition from low to high reflectance at about 2.0 μm and **b** CNiO samples showing a steep transition from low to high reflectance at about 2.5 μm

absorption bands appear to indicate the hydrophilic nature of the sol–gel synthesized silica.

The reflectance spectra for C–ZnO and C–NiO samples are presented in Fig. 3a. An attempt has been made to check reproducibility of the samples of both types by maintaining the same deposition parameters. In Fig. 3a, the dips in the spectra between 6 and 7 μm are due to water absorption (O–H bending vibrations at 1,600 cm^{-1}) [6, 9]. The O–H bending vibrations are much weaker than the case for previously studied C–SiO_2 samples [6]; this implies a lower emittance for the C–ZnO samples. The O–H stretching vibrations around 2.7 and 3.3 μm (3,000–3,600 cm^{-1}) of the C–SiO_2 samples (see Fig. 1a) are clearly absent in the C–ZnO samples resulting in an even lower emittance (NB: a high reflectance from the sample in the IR wavelength range means a low emittance by the sample). The absorption due to the Zn–O vibrations is expected between 20 and 25 μm [10, 11], which is just beyond the measurement range for the present work. A major difference between these spectra and those of previous experiments on C-SiO_2 selective absorbers [6] is the absence of strong absorption between 2.5 and 20 μm, which signifies a great improvement in emittance characteristics of the C–ZnO absorber coatings compared with those of the previous study of C–SiO_2 selective absorbers. Another added advantage is that the UV–Vis absorption of the C–ZnO based samples seems somewhat better than that of C–SiO_2. However, a drawback of the C–ZnO based absorber surfaces is that the transition step from low to high reflectance is not steep enough for all samples investigated.

The reflectance spectra of the C–NiO samples are presented in Fig. 3b. It is clear that both modes of the O–H vibrations of the C–ZnO samples are absent in the C–NiO samples; this yields even better emittance characteristics. The step transition for all the samples is between 2 and 3 μm and is steeper than that of the C–ZnO samples. This gives the C–NiO samples the closest to a step transition at 2.5 μm expected for an ideal selective solar absorber surface for domestic water heating.

The selected area electron diffraction (SAED) result shown in Fig. 4a also demonstrated that in most regions, the coating consisted of nanocrystalline NiO. The electron diffraction reveals that there exists a small amount of Ni grains with diameter of about 30 nm in some regions of the film (see Fig. 4b).

Raman Spectroscopy

The Raman spectroscopy data of the samples were first analysed using the Tuinstra–Koenig (TK) equation. The background to this equation, which is important for Raman spectroscopy characterization of carbon allotropes, is given in a review article by Gouadec and Colomban [12]. This equation relates the ratio of phonon intensities of the disorder (defect), $I_{D,}$ and the prefect graphite peak, I_G, to the carbon allotrope grain size. The empirically calibrated TK equation is given as:

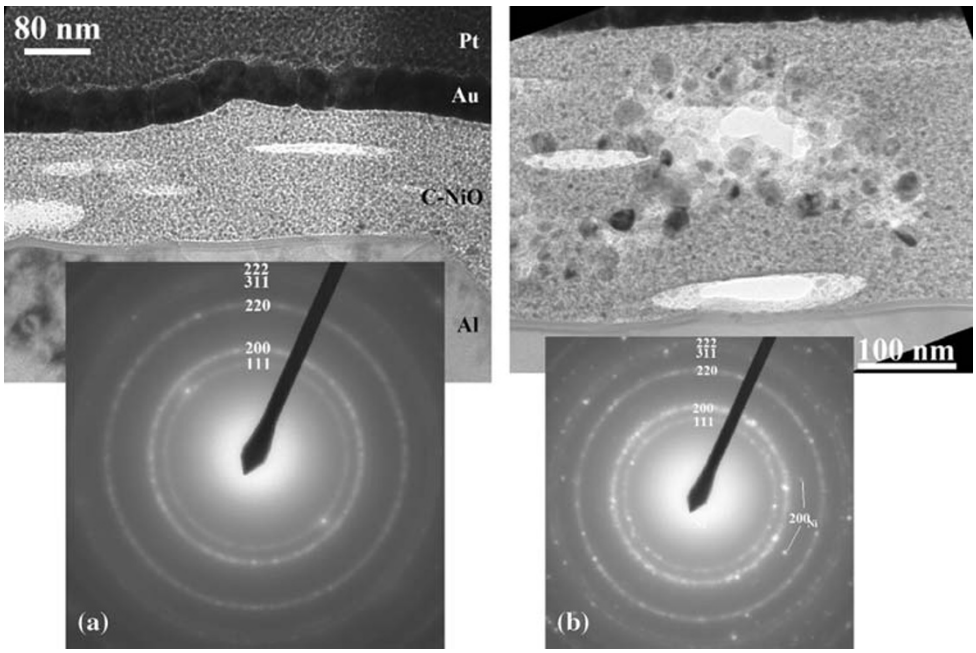

Fig. 4 **a** A TEM image together with the corresponding SAED pattern of a C–NiO sample and **b** some Ni grains in the C–NiO sample. The inset is the corresponding SAED pattern

$$\frac{I_{D(1350cm^{-1})}}{I_{G(1580cm^{-1})}} = \frac{C(\lambda)}{L_{grain}} \qquad C(\lambda = 514.5nm) = 44nm \qquad (1)$$

In our samples, the D peaks are weaker than the G peaks and this suggests that the grain sizes could be larger than 44 nm [12]. From the peak positions ω_D and ω_G and intensities I_D and I_G of the D and G-peaks, respectively, we calculated the shifts $\Delta\omega_D$ and $\Delta\omega_G$, ratio I_D/I_G, and hence the grain sizes L_{grain} and these are presented in Table 1. (It must be noted that grain size is different from the size of the crystallites that agglomerate to form the grain.)

From the calculations, it was found that in all samples, the D and G-peaks shift in position to higher Raman shift. The reason for this "blue shift" is due to compressive stress on the carbon allotrope caused by the matrix. Tensile stress leads to red-shift as shown in the following relation between the observed peak position ω_{vib} and the strain ε_{lb} of the carbon–carbon bond of length l_b given by [12]:

$$\omega_{vib} = \omega_0\left[1 - \left(\frac{a+r+3}{2}\right).\varepsilon_{lb}\right] \qquad (2)$$

Here ω_0 if the peak position for the strain-free bulk sample. The symbols a and r are, respectively, attractive and repulsive exponents in the Mie-Grunsen potentials in solids that govern the bond energies as a function of interatomic distances. (The values for a and r are respectively 6 and 12 for van der Waal's forces in the 6–12 Lennard-Jones potential, 1 and 9 for ionic bonding and $a + r = 3$ for covalent bonding.) It can be clearly seen that a positive strain (tensile strain) reduces the observed peak ω_{vib} leading to a red shift whereas a negative strain (compressive strain) leads to the opposite effect in peak position shift—a blue shift. This means that in all samples, carbon clusters are compressively strained by their respective host materials as expected.

Phonon confinement models have been used to fit the asymmetrical broadening of the Raman peaks. We assume that the carbon clusters and nanocrystallites are perfect spheres. In this case, we can fit to the Raman spectral data the following Richter et al. (1981) [13] equation for asymmetrical Raman line-shapes due to phonon confinement in nanomaterials given as:

$$I(\omega) = A_0 \int_0^\infty \frac{\exp\left(-\frac{d^2q^2}{\alpha}\right)}{[\omega - \omega(q)]^2 + \frac{\Gamma_0^2}{4}} d^3q \qquad (3)$$

In this equation, A_0 is a pre-factor to be determined from the fitting session, d is the carbon cluster size, q is the wave

Table 1 Calculations of Raman shifts and grain size estimations for the C–SiO_2, C–ZnO and C–NiO samples

Sample	ω_D (cm^{-1})	ω_G (cm^{-1})	I_D	I_G	$\omega\Delta_D$ (cm^{-1})	$\omega\Delta_G$ (cm^{-1})	I_D/I_G	L_{grain} (nm)
Carbon	1,350	1,580						
C–SiO_2	1,384.9	1,603.64	29,144.7	37,241.6	34.9	23.64	0.78,258	56.2
C–ZnO	1,362.6	1,594.3	2,207.96	2,923.4	12.6	14.3	0.75527	58.3
C–NiO	1,358.9	1,594.3	1,435.87	2,009.8	8.9	14.3	0.71443	61.6

vector of the exciting light source in the Raman spectroscopy set-up, α is the scaling factor, $\omega(q)$ is the phonon dispersion relation for the material under study and Γ_0 is the full width at half maximum of the Raman line-shape for bulk form of the same material. For materials of different shapes, a modification of the d^3q is required. For instance, d^3q becomes $2\pi qdq$ for nanorods [14] and proportional to q^2dq for quantum dots [15].

The typical Raman spectroscopy plots are presented in Figs. 5–7 for vibrational properties of carbon in SiO_2, ZnO and NiO, respectively. No significant asymmetry was observed in the D peak in all samples. This means that the size of the defect in these carbon clusters is large. However, asymmetry in the G peak was observed in all samples indicating that the nano-carbon is graphitic in structure.

In Figs. 5–7, we have re-drawn the G peak in a separate graph in order to demonstrate this asymmetry. The Richter equation was fitted to the experimental data and the relevant parameters in this equation were extracted. The results

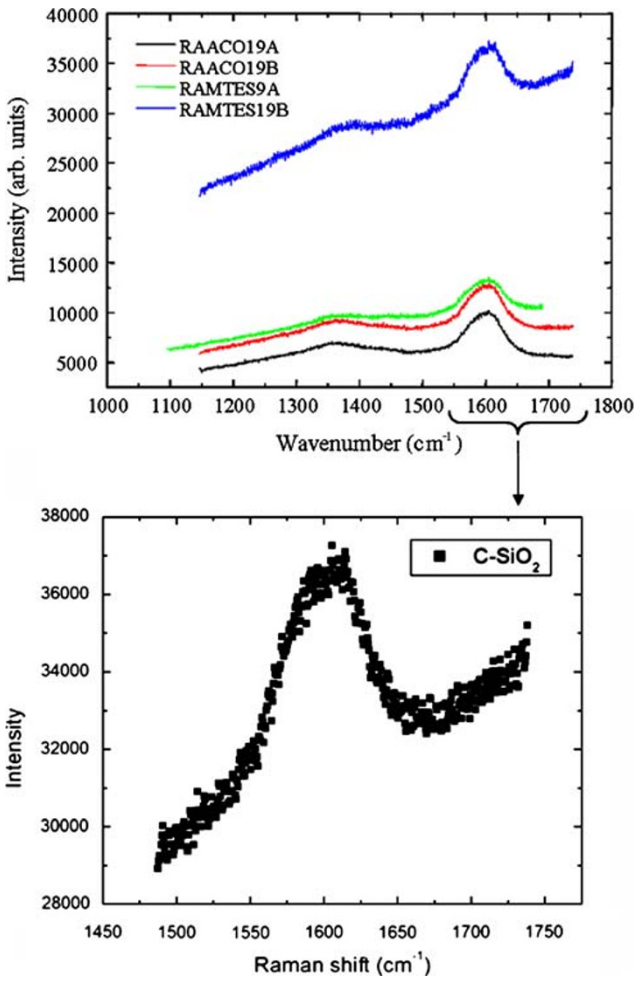

Fig. 5 Raman spectroscopy on difference spots of the C–SiO_2 sample. The G peak has been re-drawn to show the increasing background noise especially at high scattering intensities

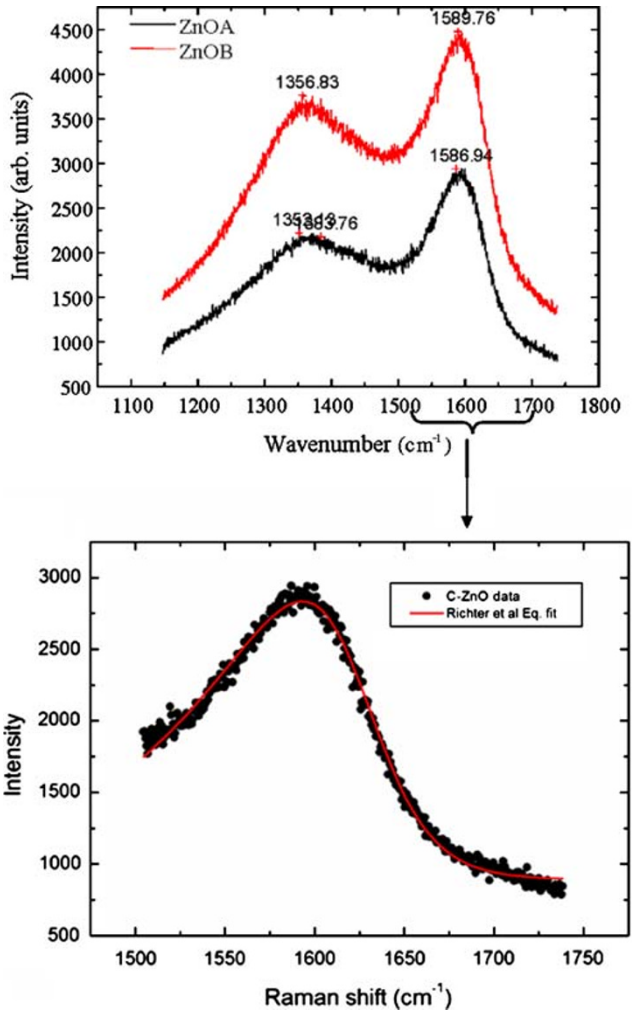

Fig. 6 Raman spectroscopy on difference spots of the C–ZnO sample. The G peak has been re-drawn to show the asymmetry which is an indication of the phonon confinement in nanoclusters of carbon within the ZnO matrix

for C–NiO and C–ZnO samples are similar except that intensity is higher in ZnO than NiO. It is interesting to note that the C–SiO_2 sample shows completely different results: extremely high scattering intensity and an increasing background intensity as the Raman shift increases. Due to the increasing background intensity, the phonon confinement model could not be used for the C–SiO_2 samples. Typical parameters for the best C–NiO sample are tabulated in Table 2. It can be seen that the crystallite size that is responsible for the observed asymmetry in the Raman spectral line-shape for carbon in NiO is 6 nm.

Conclusions and Comments

We have been able to study C–SiO_2, C–ZnO and C–NiO selective solar absorber materials using FTIR and Raman

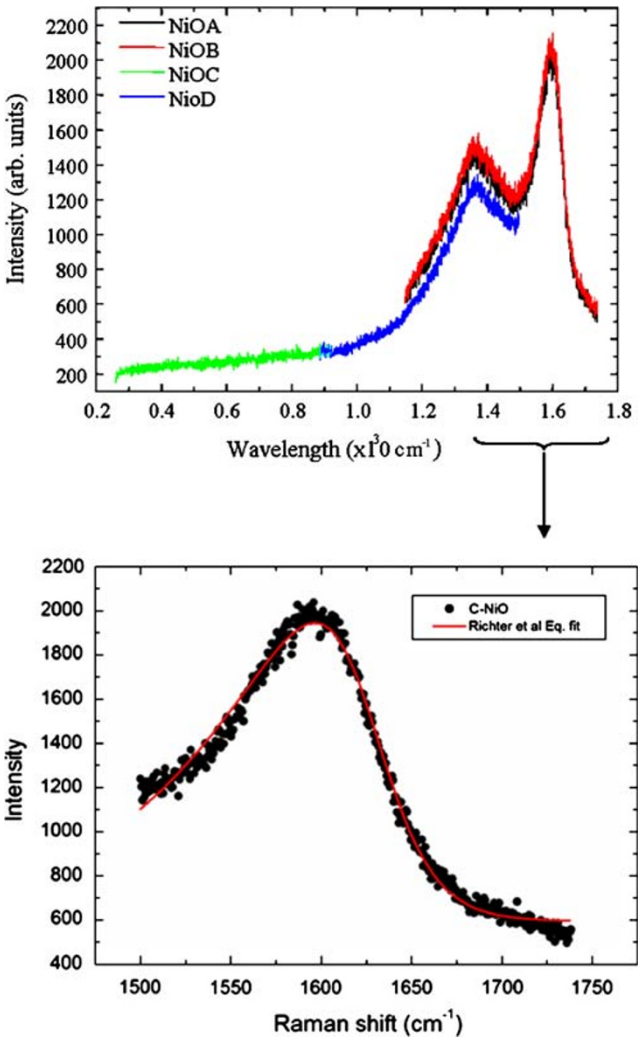

Fig. 7 Raman spectroscopy on difference spots of the C–NiO sample. The G peak has been re-drawn to show that the carbon clusters are nanostructures as indicated from the asymmetry of this peak

spectroscopy techniques. The thermal emittances of the samples were 10% for C–SiO_2, 6% for the C–ZnO and 4% for the C–NiO samples. The solar absorptances were 95%, 71% and 84% for the C–SiO_2, C–ZnO and C–NiO samples, respectively. Based on these results, C–NiO samples proved to have the best solar selectivity behaviour followed by the C–ZnO, and last were the C–SiO_2 samples.

Table 2 Values extracted from the Richter equation fitting of the C–ZnO and C–NiO samples

Parameters in phonon confinement model	Extracted values
FWHM (bulk + broadening)	80 cm^{-1}
Scale parameter	0.081
Crystallite size	6 nm
Pre-factor A_0	7/8,000
Background noise in intensity	1,000
Lattice parameter a_0 in graphite	0.25 nm
Dispersion constant	14 cm^{-2}

The Raman analysis of the selective solar absorber samples has shown that carbon behaves differently when placed in matrices of SiO_2, ZnO and NiO. In all matrices, the D-band is broad but has no significant asymmetry. The G-band is indeed asymmetrically broadened in all cases. The ratio of the intensities of these phonon peaks yields the following grain sizes for the carbon clusters in the matrices, respectively: 56.2 nm, 58.3 nm and 61.6 nm. The difference in the grain sizes may be said to be insignificant. Using the phonon confinement model of Richter [13] yields a crystallite size of 6 nm which is responsible for the asymmetrical broadening for both the C–NiO and C–ZnO samples. The C–NiO samples have the least scattering intensity of the three. The highest scattering was observed in C–SiO_2 samples. It was not possible to analyse the C–SiO_2 samples due to the rising background intensity as the Raman shift increased.

Acknowledgements Rudolf Erasmus of Witwatersrand University, South Africa, kindly assisted with the Raman experiments. The CSIR-National Laser Centre provided financial assistance.

References

1. X. Niu, W. Zhang, E. Zhang, J. Sun, G. Lu, J. Cryst. Growth **263**, 167 (2004)
2. S.L. Howell, K.C. Gordon, J. Raman Spectrosc. **39**, 813 (2008)
3. F. Froment, A. Tournie, P. Colomban, J. Raman Spectrosc. **39**, 560 (2008)
4. R.L. Frost, J. Cejka, M.J. Dickfos, J. Raman Spectrosc. **39**, 779 (2008)
5. M.D. Hargreaves, K. Page, T. Munshi, R. Tomset, G. Lynch, H.G.M. Edwards, J. Raman Spectrosc. **39**, 873 (2008)
6. G. Katumba, J. Lu, L. Olumekor, G. Westin, E. Wäckelgård, J. Sol–Gel Sci. Technol. **36**, 33 (2005)
7. G. Katumba, L. Olumekor, A. Forbes, G. Makiwa, B. Mwakikunga, J. Lu, E. Wackelgard, Sol. Energ. Mater. Sol. C. **92**, 1285 (2008)
8. W. Que, Y. Zhou, Y.L. Lam, Y.C. Chan, C.H. Kam, Thin Solid Films **358**, 16 (2000)
9. A.V. Rao, R.R. Kalesh, G.M. Pajonk, J. Mater. Sci. **38**, 4407 (2003)
10. X.-W. Du, Y.-S. Fu, J. Sun, X. Han, J. Liu, Semicond. Sci. **21**, 1202 (2006)
11. M. Matsumura, Z. Bandic, R.P. Camata, Mater. Res. Soc. Symp. Proc. **869**, D1.7.1 (2005)
12. G. Gouadec, Ph. Colomban, Prog. Cryst. Growth Charact. Mater. **53**, 1 (2007)
13. H. Richter, Z.P. Wang, L. Ley, Solid State Commun. **39**, 625 (1981)
14. B.W. Mwakikunga, E. Sideras-Haddad, A. Forbes, C. Arendse, Phys. Stat. Sol. (a) **205**, 150 (2008)
15. S. Piscanec, M. Cantoro, A.C. Ferrari, J.A. Zapien, Y. Lifshift, S.T. Lee, S. Hoffmann, J. Robertson, Phys. Rev. **B 68**, 241312(R) (2003)